JOURNAL OF Materials CHEMISTRY

Syntheses, crystal structures and magnetic properties of francisite compounds $Cu_3Bi(SeO_3)_2O_2X$ (X = Cl, Br and I)

P. Millet,*[a] B. Bastide,[a] V. Pashchenko,[b,c] S. Gnatchenko,[c] V. Gapon,[c] Y. Ksari[d] and A. Stepanov[d]

[a]*Centre d'Elaboration de Matériaux et d'Etudes Structurales, CNRS, 29 rue Jeanne Marvig, BP 4347 Toulouse Cedex 4, France. E-mail: millet@cemes.fr*
[b]*Grenoble High Magnetic Field Laboratory, MPI-FKF and CNRS, 38042 Grenoble Cedex 9, France*
[c]*B. Verkin Institut for low Temperature Physics and Engineering, National Academy of Sciences of Ukraine, 47 Lenin Avenue, 61164 Kharkov, Ukraine*
[d]*Laboratoire Matériaux et Microélectronique de Provence, Université d'Aix-Marseille III and CNRS, Faculté des Sciences de Saint-Jérôme, C-151, 13397 Marseille Cedex 20, France*

Received 2nd October 2000, Accepted 8th January 2001
First published as an Advance Article on the web 16th February 2001

Synthetic analogues of francisite, a mineral of complex formula $Cu_3Bi(SeO_3)_2O_2X$ with X = Cl, Br, I, have been obtained by solid state reaction. Contrary to the previous structure description, the framework can be better described as formed of copper(II)–oxygen layers linked together in the [001] direction by long bismuth–oxygen bonds. These layers are formed by a hexagonal network of $[CuO_4]$ square plane sharing apices whose geometry is reminiscent of a Kagomé type lattice. Preliminary magnetic susceptibility measurements performed on the X = Cl and Br compounds have revealed ferromagnetic-like behaviour below $T_c \approx 24$ K. Linear birefringence and X-band Electron Spin Resonance (ESR) data are also presented.

I. Introduction

In the search for materials potentially interesting as low dimensional quantum magnets, few copper(II) oxychlorides have been studied owing to the fact that they present a structure similar to those of high T_c superconductors. Let us mention as examples $Ba_2Cu_3O_4Cl_2$ [1] which presents a layered structure composed of Cu_3O_4 planes, and $Sr_2CuO_2Cl_2$ which, with the same type of copper–oxygen plane, is the paradigm 2D spin-1/2 Heisenberg antiferromagnet.[2]

Our strategy to obtain low dimensional compounds has been to substitute the so-called lone pair cations, such as Se(IV), which are assumed to act as chemical scissors, for the alkaline-earth elements. Note that the chemistry of such systems has not been widely studied with only one known oxide compound of copper(II) and selenium(IV), $Cu_5Se_2O_8Cl_2$.[3] In the ternary phase diagram CuO–$CuCl_2$–SeO_2, we recently isolated two new compounds, $Cu_9O_2(SeO_3)_4Cl_6$ [4] and $Cu_3(SeO_3)_2Cl_2$.[5] Interestingly, natural homologues of the former two compounds have been extracted from the exhalations of Tolbachick volcano, Kamchatcka, Russia.[6,7] However the main concern regarding these compounds is that their crystal structures are quite complicated with at least three different copper(II) coordination polyhedra. While looking for simpler structures we found a paper by Pring, Gatehouse and Birch[8] describing the X-ray single-crystal structure of a copper bismuth oxychloro selenite of formulae $Cu_3Bi(SeO_3)_2O_2Cl$, which was called francisite, from Iron Monarch, South Australia, and in which the two different copper(II) ions, in square planar arrangement, make a peculiar hexagonal like network of Cu–O bonds (see Fig. 1). This paper presents the synthesis and crystal structure determinations of synthetic analogues of francisite $Cu_3Bi(SeO_3)_2O_2X$ (X = Cl, Br, I). Experimental data obtained by static and ac susceptibility, X-band electron spin resonance and optical measurements are also presented.

II. Synthesis

Homogeneous powders of synthetic francisite were obtained starting from the following mixtures: 5 CuO : 4 SeO_2 : 1 $CuCl_2$ or $CuBr_2$: 1 Bi_2O_3 for $Cu_3Bi(SeO_3)_2O_2X$ (X = Cl, Br) and 5 CuO : 4 SeO_2 : 1 Cu : 1 I_2 : 1 Bi_2O_3 for the iodine containing compound. The mixtures were introduced into Pyrex tubes which were sealed under primary vacuum and then heated at

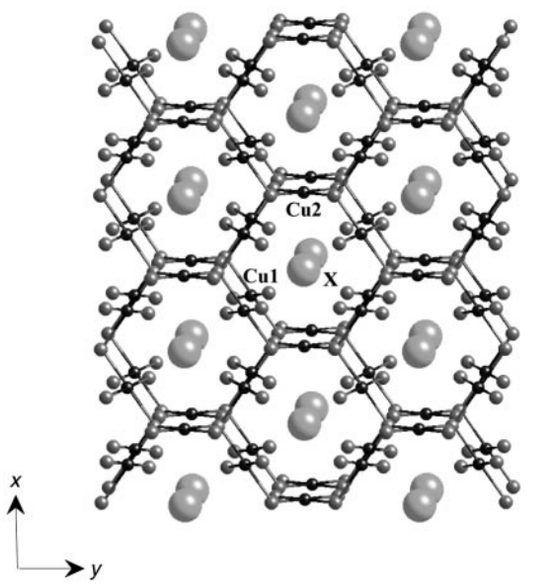

Fig. 1 The hexagonal network made of $[CuO_4]$ square planes sharing apices in the [001] and [010] directions. The large grey spheres correspond to the halide ions located inside the tunnels parallel to the [001] direction.

 DOI: 10.1039/b007920k

Table 1 Summary of the data collection and refinement data for $Cu_3Bi(SeO_3)_2O_2X$ (X = Cl, Br, I) structures

Formula	$Cu_3Bi(SeO_3)_2O_2Cl$	$Cu_3Bi(SeO_3)_2O_2Br$	$Cu_3Bi(SeO_3)_2O_2I$
M_r	720.97	765.43	812.42
Crystal system	orthorhombic	orthorhombic	orthorhombic
Space group	*Pmmn*	*Pmmn*	*Pmmn*
a/Å	6.3540(4)	6.3900(3)	6.4360(2)
b/Å	9.6350(5)	9.6940(4)	9.7510(4)
c/Å	7.2330(4)	7.2870(3)	7.3770(3)
V/Å^3	442.81(4)	451.39(3)	462.96(3)
Z	2	2	2
F(000)	638	674	710
Temperature/K	293(2)	293(2)	293(2)
D_c/Mg m^{-3}	5.4074	5.632	5.828
μ/cm^{-1}	354.54	209.42	198.74
Crystal colour	green	dark green	pink
Crystal habit	square plate	square plate	square plate
Crystal size/mm	$0.122 \times 0.058 \times 0.016$	$0.106 \times 0.064 \times 0.032$	$0.100 \times 0.090 \times 0.011$
Wavelength/Å	0.71069	0.56230	0.56230
2θ/°	2.82 to 31.03	2.21 to 43	2.18 to 38.5
Reflections collected	6287	8084	13452
Data/restraints/parameters	755/0/47	870/0/47	898/0/47
R (%)	2.81	3.13	2.31
R_W (%)	5.67	7.91	5.44
Goodness-of-fit on F^2	1.345	1.070	1.116
Weighting scheme, 2 terms Chebychev	0.0001/3.7577	0.0447/1.3193	0.0211/1.1216
Largest diff. peak and hole/e Å^{-3}	1.981/−2.859	2.940/−3.657	1.418/−2.414

400 °C for 24 hours. Single crystals could be obtained from the same mixtures after thermal treatment at 550 °C for 36 hours followed by slow cooling (5 °C h^{-1}) to room temperature. Plate-like crystals suitable for the single crystal X-ray diffraction study were isolated from the bulk materials. Data were collected on an Enraf-Nonius four circle diffractometer equipped with a KAPPA-CCD detector. The cell parameters were determined from the collection of ten frames using the program Collect.[9] SIR92[10] was used to solve the structures by direct methods. Structures were refined using SHELXL-97.[11] An absorption correction was applied during the structure refinement using the program SORTAV.[12] The set of physical and crystallographic characteristics as well as the experiment conditions are listed in Table 1. Owing to the different wavelengths used in these experiments and in order to get approximately the same number of reflections in the three cases the reflections outside the resolution range 0.665 Å in the bromide and iodide phases were not used in the refinement.

CCDC reference number 1145/272. See http://www.rsc.org/suppdata/jm/b0/b007920k/ for crystallographic files in .cif format.

III. Crystal structure

In the following CBSX will be used instead of $Cu_3Bi(SeO_3)_2O_2X$. The three phases corresponding to X = Cl, Br and I are isostructural. The atomic parameters and selected interatomic distances are listed in Table 2 and Table 3 respectively. These structural data agree well with the previous structural determination by Pring, Gatehouse and Birch.[8]

As previously mentioned, Cu1 and Cu2 are in square planar coordination with classical copper(II)–oxygen bonds in the range 1.933–1.978 Å. These square planes share apices to form, as indicated in Fig. 1, copper–oxygen layers, the geometry of which is reminiscent of a Kagomé type lattice. A projection of the CBSX crystal structure along the [100] direction, in Fig. 2, clearly shows that the copper–oxygen layers (represented as dark gray waves) are linked together in the [001] direction by only long bimuth(III)–oxygen bonds, represented as thick black sticks: for the three phases, Bi–O3 bonds are over 2.8 Å. Interestingly the main structural modification induced by the chlorine atom substitution by bigger anions such as Br^- and I^- is the increase of these Bi–O3 bonds; 2.854(3) Å and 2.955(2) Å in the compounds with Br and I respectively compared to 2.821(2) for the Cl one. The fact that the Bi–halogen distances follow the same evolution with the halogen substitution (see Table 3) suggests that this structural modification is a direct consequence of the halogen–bismuth lone pair interaction in the tunnel. The bigger anions Br^- and I^- repel the bismuth lone pair and a concomitant increase of the Bi–O3 bond is

Table 2 Final atomic coordinates and equivalent isotropic displacement parameters for $Cu_3Bi(SeO_3)_2O_2X$ (X = Cl, Br, I) structures. $U_{eq} = (1/3)\ \Sigma_i\Sigma_j U_{ij} a_i a_j \boldsymbol{a}_i.\boldsymbol{a}_j$

		$Cu_3Bi(SeO_3)_2O_2Cl$	$Cu_3Bi(SeO_3)_2O_2Br$	$Cu_3Bi(SeO_3)_2O_2I$
Bi	x	1/4	1/4	1/4
	y	1/4	1/4	1/4
	z	0.24120(5)	0.24012(4)	0.23653(3)
	U_{eq}/Å^2	0.0094(1)	0.0085(1)	0.0103(1)
Se	x	1/4	1/4	1/4
	y	0.55698(7)	0.55649(6)	0.55601(6)
	z	0.60975(9)	0.61157(9)	0.61693(7)
	U_{eq}/Å^2	0.0094(1)	0.0085(1)	0.0103(1)
Cu1	x	0	0	0
	y	0	0	0
	z	0	0	0
	U_{eq}/Å^2	0.0156(2)	0.0127(2)	0.0129(2)
Cu2	x	1/4	1/4	1/4
	y	1/4	1/4	1/4
	z	0.7920(2)	0.7925(2)	0.7940(1)
	U_{eq}/Å^2	0.0094(1)	0.0132(2)	0.0103(1)
X	x	1/4	1/4	1/4
	y	3/4	3/4	3/4
	z	0.1496(5)	0.1579(2)	0.17049(7)
	U_{eq}/Å^2	0.0420(9)	0.0224(3)	0.0164(1)
O1	x	1/4	1/4	1/4
	y	0.1141(5)	0.1138(5)	0.1144(4)
	z	0.9922(6)	0.9916(6)	0.9928(5)
	U_{eq}/Å^2	0.011(1)	0.0089(8)	0.0101(7)
O2	x	0.0427(7)	0.0410(7)	0.0427(5)
	y	0.5828(5)	0.5836(5)	0.5839(4)
	z	0.7547(5)	0.7558(5)	0.7588(4)
	U_{eq}/Å^2	0.0202(9)	0.0169(8)	0.0164(6)
O3	x	1/4	1/4	1/4
	y	0.1162(6)	0.1159(5)	0.1157(5)
	z	0.5882(7)	0.5897(7)	0.5952(5)
	U_{eq}/Å^2	0.022(1)	0.019(1)	0.0180(8)

Table 3 Selected interatomic distances (Å) for $Cu_3Bi(SeO_3)_2O_2X$ (X = Cl, Br, I) structures

	$Cu_3Bi(SeO_3)_2O_2Cl$	$Cu_3Bi(SeO_3)_2O_2Br$	$Cu_3Bi(SeO_3)_2O_2I$
Bi–O1 (×2)	2.226(5)	2.240(6)	2.231(4)
Bi–O2 (×4)	2.460(4)	2.461(5)	2.485(3)
Bi–O3 (×2)	2.821(2)	2.854(3)	2.955(2)
Cu1–O1 (×2)	1.933(3)	1.942(3)	1.959(2)
Cu1–O2 (×2)	1.964(3)	1.977(4)	1.978(3)
Cu2–O1 (×2)	1.952(5)	1.964(6)	1.975(4)
Cu2–O3 (×2)	1.959(5)	1.971(6)	1.967(4)
Se–O3	1.676(6)	1.680(6)	1.682(4)
Se–O2 (×2)	1.702(4)	1.717(5)	1.717(3)
Cu1–Cu1	3.177(1)	3.195(1)	3.218(1)
Cu1–Cu2	3.254(1)	3.273(1)	3.292(1)
Bi–X	4.252(1)	4.315(1)	4.400(1)
Cu1–X	3.081(1)	3.122(1)	3.180(1)
Cu2–X	3.205(1)	3.215(1)	3.228(1)

observed leading to copper–oxygen layers moving further apart as outlined by the arrows in Fig. 2.

The selenium atoms are three-fold coordinated to three copper–oxygen square planes of the same copper–oxygen layer, with Se–O distances which do not vary from one phase to the other. The stereochemically active lone pair of Se (denoted E1), which is located in the tunnels, completes the selenium coordination polyhedron to form a tetrahedron.

IV. Magnetic properties

A. Experimentation

The static and ac susceptibility of CBSCl and CBSBr samples have been measured using Oxford Instruments Maglab equipment. The measurement system is a standard ac susceptibility bridge providing an estimated sensitivity of 10^{-8} emu. The oppositely wound secondary coils can be used to measure the magnetic moment of a sample in the presence of an applied static field. In the latter case, the voltage induced through these compensated coils is measured with a Keithley 2001 voltmeter during the extraction of the sample. The magnetic moment (proportional to the integrated voltage) was obtained after calibration of the system with a pure nickel sample. A magnetic moment as small as $\sim 10^{-5}$ emu can be detected with this experimental setup. The polycrystalline samples which had a typical mass of 50 mg were placed in 4 mm diameter Pyrex tubes filled with helium gas. The samples were first cooled from room temperature to 1.8 K at a sweep rate of ~ 3 K min^{-1}. Successively, the field was then slowly raised from 0 to 10 kG, the superconducting magnet set in the persistent mode and the acquisition launched. The temperature was then raised from 1.8 to 300 K at a sweep rate of 0.7 K min^{-1} while recording the data, except for the χ_{ac} experiment on CBSBr for which the measurements were made during the cooling of the sample at 0.7 K min^{-1}. χ_{ac} data were obtained using a 1 kHz excitation field with a peak amplitude of 20 G. No static field was applied in ac susceptibility experiments.

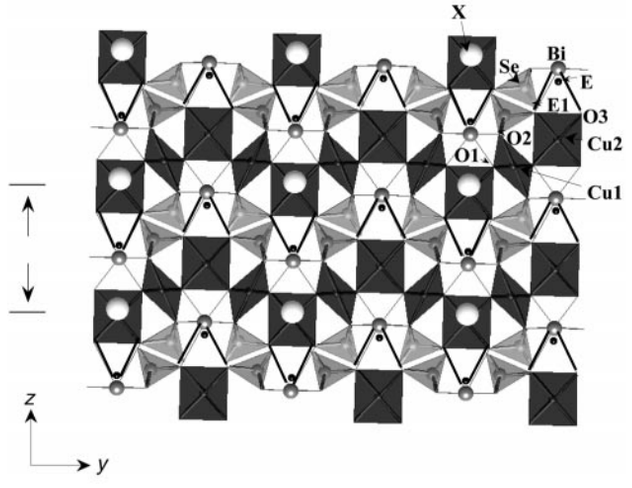

Fig. 2 Projection of CBSX along the [100] direction. Cu(II)–O square planes are in dark gray, Se tetrahedral coordination polyhedra, [SeO_3E1], in gray, halogen X as white circles, and Bi(III) as dark gray circles with its lone pair E as a small black circle. Bi–O3 bonds are represented as thick black sticks. The direction of displacement of Cu–O layers upon chlorine substitution is indicated by the arrows.

B. Results

Fig. 3 shows the temperature variation of the magnetic susceptibility of a CBSCl sample obtained using this experimental procedure. The curve presents a sharp maximum at $T_c = 23.5(5)$ K. Above this temperature, the susceptibility follows a Curie–Weiss (CW) law $\chi = C/(T-\theta)$. The inset of Fig. 3 shows that two sets of parameters θ_1, C_1 and θ_2, C_2, corresponding to the high and low temperatures respectively, can be determined. Above ~ 150 K, χ is characterised by a ferromagnetic Weiss temperature $\theta_1 = 57(2)$ K and a Curie constant $C_1 = 0.370(5)$ cm^3 K (Cu mol)$^{-1}$, implying an average effective moment $\mu_{eff1} = 1.72(5)$ μ_B per Cu atom and an average g-factor $\langle g_1 \rangle = 2.0(1)$. μ_{eff1} is almost equal to 1.73 μ_B, the value corresponding to a $S = 1/2$ spin system. Between 35 and ~ 150 K, $1/\chi(T)$ still behaves linearly but the slope of the curve is smaller than the one measured above 150 K. $\chi(T)$ obeys in this temperature range a CW law characterised by the parameters $\theta_2 = 20(2)$ K and $C_2 = 0.506(5)$ cm^3 K (Cu mol)$^{-1}$ implying $\mu_{eff2} = 2.02(5)$ μ_B per Cu atom and $\langle g_2 \rangle = 2.3(1)$.

Fig. 4 shows that the susceptibility of a CBSBr sample behaves qualitatively in the same way except that below $T_c = 24.2(5)$ K, $\chi(T)$ is almost temperature independent and displays a small anomaly at 6.7 K. Between 150 and 300 K, $\chi(T)$ can be parameterised by $\theta_1 = 51(2)$ K, $C_1 = 0.338(5)$ cm^3 K (Cu mol)$^{-1}$ implying $\mu_{eff1} = 1.64(5)$ μ_B and $\langle g_1 \rangle = 1.9(1)$. From 150 K to 35 K, $\chi(T)$ is characterised by $\theta_2 = 26(2)$ K, $C_2 = 0.419(5)$ cm^3 K (Cu mol)$^{-1}$, $\mu_{eff2} = 1.83(5)$ μ_B and $\langle g_2 \rangle = 2.1(1)$.

On the basis of these experimental results, CBSCl and CBSBr are paramagnets above 23.5 K and 24.2 K respectively. However the change of $\langle g \rangle$ evidenced around $T_o \sim 150$ K from the CW law analysis is striking and rather unusual. For

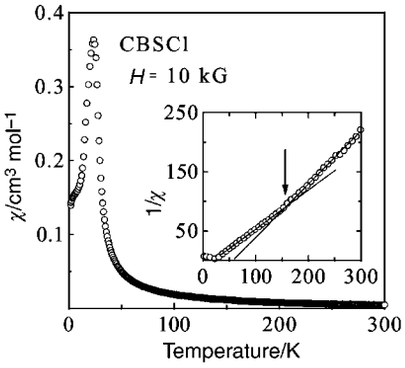

Fig. 3 Magnetic susceptibility χ of a CBSCl powder sample. Inset: plot of $1/\chi$, the vertical arrow delimits the two temperature regions characterized by a specific linear behaviour. The continuous lines are the linear fits from which the parameters, in the text, have been deduced.

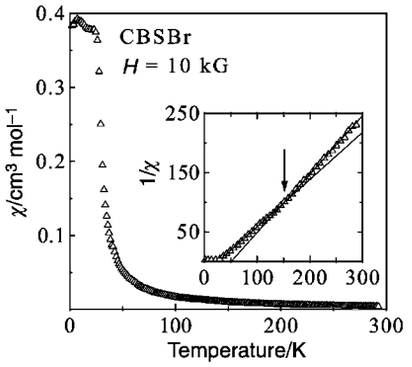

Fig. 4 The same as in Fig. 3 but for CBSBr.

example, a relative change $\Delta\langle g\rangle/\langle g\rangle \sim 15\%$ at T_o in the case of CBSCl implies an important modification of the electric field surrounding the Cu^{2+} ions. Thus, a change of the distances between a given Cu^{2+} ion and its nearest neighbors probably occurs at this temperature. The variation of the Weiss temperature, θ, at T_o would then simply reflects the modification of the (or some) Cu–Cu exchange integrals. These features made us think that a structural phase transition may exist near T_o. In order to further investigate the possible origin of this unusual behaviour, we performed low field ac susceptibility measurements. Fig. 5 shows a typical curve obtained with the CBSCl sample used in static susceptibility experiments. When the temperature is raised from 1.8 K, the real part χ'_{ac} first increases, passes through a sharp maximum at $T_c^* = 26.7(5)$ K and then decreases rapidly. It is interesting to note that the curve representing χ'_{ac} displays an anomaly in the temperature region where a change of slope of the reciprocal static susceptibility is evidenced. As can be seen in the inset of Fig. 5, this anomaly occurs at 133 ± 10 K and 123 ± 10 K for CBSCl and CBSBr respectively and it is much more pronounced in the case of CBSBr. In order to correlate these magnetic anomalies with the structural properties of these materials, we have also performed optical measurements which are detailed in the following section.

V. Linear birefringence

A. Experimentation

The temperature dependence of the linear birefringence Δn was measured on a small crystal of CBSCl between 25 and 280 K by the compensation technique using a quarterwave plate. The light source was a He–Ne laser ($\lambda = 633$ nm). The light beam, linearly polarized parallel to the [011] axis, is directed along the [100] orthorhombic axis of the crystal. In the case $\Delta n = n_b - n_c$, where n_b and n_c are the refractive indices of the crystal along the

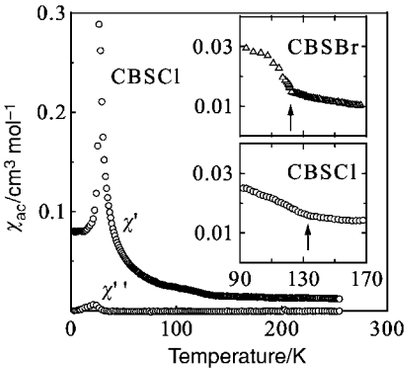

Fig. 5 Real (χ') and imaginary (χ'') parts of the ac susceptibility of CBSCl. Insets: zooms of the temperature region where a χ' anomaly was evidenced for CBSBr and CBSCl.

b and c axes respectively. The output light beam is affected by this difference and becomes therefore elliptically polarized. To compensate the phase difference δ between the linearly polarized eigenmodes of the crystal, a quarterwave plate was used as the compensator. The fast (or slow) axis of the quarterwave plate was parallel to the polarization plane of incident light and the [011] axis of the crystal. In this way, we transformed the elliptically polarized light into linearly polarized light with the polarization plane rotated by angle $\delta/2$. Measuring this angle, we defined the phase difference δ as well as the linear birefringence from the relation

$$\Delta n = (\delta\lambda)/(360d) \quad (1)$$

where d is the sample thickness. The modulation of the light beam on the polarization plane was used to measure the angle of the polarization plane rotation $\delta/2$. To define the value of the linear birefringence, measurements of δ were carried out on several single crystal samples of different thickness at room temperature. Plates of thickness of about 35, 50, 70, 90, and 100 μm were used for these measurements. The dimensions of the sample did not exceed several hundred micrometers. The thickness of the sample was measured by means of optical microscopy. The value of the linear birefringence of CBSCl is equal to $(2.5 \pm 0.3) \times 10^{-3}$ at room temperature. The measurement accuracy of the linear birefringence is essentially determined by the accuracy of the sample thickness which is not high due to the very small sample size. Finally, the temperature dependence of the linear birefringence was measured in the 100 μm thickness sample. This one was placed in a helium cryostat. A copper–constantan thermocouple was used as the temperature sensor.

B. Results

The temperature dependence of the linear birefringence obtained for a CBSCl single crystal is shown in Fig. 6. Δn increases as the temperature decreases from 280 K to 115 K. Usually the temperature change of the linear birefringence is related to the variation of the crystal lattice parameters. In the temperature region under consideration, a linear temperature dependence of $\Delta n(T)$ is observed. A rapid decrease of Δn is found below 110 K. This change of behaviour of $\Delta n(T)$ can be related to a structural phase transition. If a structural phase transition really occurs at $T \approx 110$ K then it is rather a second-order one because a jump of Δn is not observed experimentally. Moreover, an inhomogeneous two-phase state characterizing a first-order phase transition was not found in the vicinity of $T = 110$ K using visual observation. Usually a second-order phase transition is accompanied by a change of crystal symmetry. It should be noted that if the symmetry of the crystal becomes lower below 110 K then it apparently changes in the frame of orthorhombic symmetry. We did not find any rotation of the optical index at $T < 110$ K although the rotation of index axes should accompany a transition from ortho-

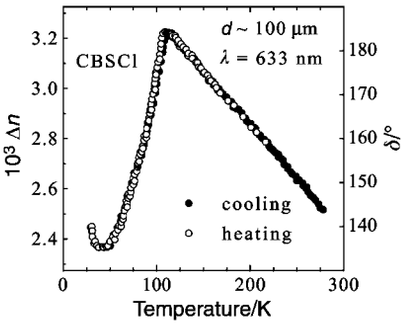

Fig. 6 Temperature dependence of the linear birefringence of a small CBSCl single crystal.

rhombic to monoclinic symmetry. Hence, either the angle of index rotation is very small (less than 1°) or the symmetry of the crystal changes in the frame of orthorhombic symmetry. We did not observe the formation of a twin domain structure that should accompany a structural phase transition with symmetry lowering from orthorhombic to monoclinic.

The upturn of the linear birefringence observed below 50 K could be related to a magnetic ordering process. Usually, the magnetic contribution in the linear birefringence contains a part related to the long-range magnetic order and one related to the magnetic fluctuations. In an antiferromagnet, the linear birefringence due to long-range magnetic order is proportional to the square of the sublattice magnetic moment and becomes equal to zero at the Néel temperature T_N. The fluctuation's contribution to the magnetic linear birefringence, which is due to the short-range magnetic order, has a maximum at $T=T_N$ and decreases on both sides of this temperature. This point in CBSCl should be verified in future experiments.

VI. Electron spin resonance

A. Experimentation

ESR spectra have been obtained between 10 and 300 K using a Bruker ESP300 spectrometer operating at $\nu=9.44$ GHz. The samples were placed at the center of a rectangular cavity excited in the TE_{102} mode. Temperature stabilization was ensured by an Oxford Instruments ITC4 controller. A standard AuFe/Cr thermocouple was used in these experiments as the temperature sensor.

We have studied powder and single crystal samples of CBSCl and CBSBr compounds. The powder samples used for the ESR experiments were the ones used in magnetic measurements and they were conditioned in the same Pyrex tubes. The small single crystals were glued with a small amount of Apiezon grease on the extremity of a thin rectangular Suprasil plate ($\sim 4\times 20$ mm^2). The other extremity of the plate was screwed to the bottom of a longer plexiglass rod. The as-made sample holder allows the crystal to be positioned in the zone of maximum microwave field amplitude without obtaining unwanted signals.

B. Results

No ESR signal from the Cu^{2+} ions belonging to the magnetic lattice was detected at any temperature in the case of the small

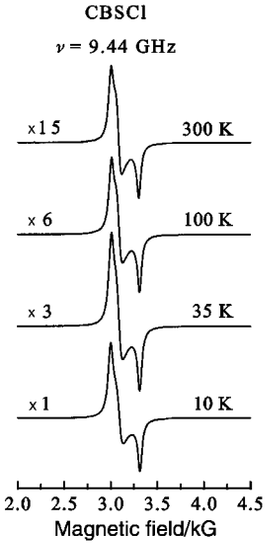

Fig. 7 Typical ESR spectra obtained at $\nu=9.44$ GHz with a CBSCl powder sample. The numbers above each curve are the scaling factor (left side) and the temperature (right side).

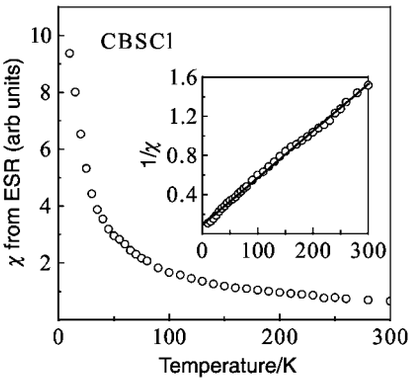

Fig. 8 Absorption intensity of a CBSCl powder sample deduced from the double integrated ESR curves. Inset: plot of $1/\chi$. The solid line is a data fit to the Curie–Weiss law ($\theta_{ESR}=-18\pm 2$ K).

CBSCl single crystals used in optical measurements. The CBSCl powder sample gives an anisotropic spectrum typical of Cu^{2+} ions in a low symmetry environment. As can be seen in Fig. 7, its shape is temperature independent over the range 10–300 K. In this figure, the spectra have been rescaled so that they have approximately the same peak to peak amplitude. The scaling factor is indicated on the left of each spectrum. The line shape at 10 K can be well fitted by the following anisotropic parameters: $g_x=2.218$, $g_y=2.180$, $g_z=2.036$; $\Delta H_x=38$ G, $\Delta H_y=60$ G, $\Delta H_z=31$ G. The susceptibility obtained by a double integration of the ESR spectra is also shown in Fig. 8. The data of Fig. 8 correspond to paramagnetic behaviour with a Weiss temperature $\theta_{ESR}\sim -18(2)$ K indicative of antiferromagnetic correlations. Since macroscopic magnetic measurements show that the susceptibility above $T_c=23.5$ K is rather characteristic of ferromagnetic correlations, we ascribe the ESR signal coming from CBSCl powder to a small amount of impurity phase or crystal defects. In order to gain a rough estimate of the number of spins effectively contributing to this ESR signal, we calibrated the spectrometer at 300 K with a weighted sample of the paramagnetic salt $CuSO_4\cdot 5H_2O$. This salt appears very convenient for such a test because the ESR signal of Cu^{2+} in $CuSO_4\cdot 5H_2O$ and that detected using the CBSCl sample have linewidths of comparable magnitude. At 300 K, the average susceptibility per spin of CBSCl is ~ 1.25 times greater than that of $CuSO_4\cdot 5H_2O$ because the magnetic correlations are predominantly ferromagnetic in CBSCl ($\theta_1=57$ K, see above). Taking this factor into account, we have found that the measured ESR intensity of the CBSCl sample represents only 5% of the expected value at 300 K confirming the extrinsic nature of the paramagnetic signal. Thus, the CBSCl phase is ESR silent at $\nu=9.44$ GHz.

Fig. 9 shows the ESR spectra obtained with a CBSBr powder sample. Here again, the spectra have been rescaled so that they have approximately the same peak to peak amplitude. The numerical factor by which each spectrum has been multiplied is indicated in the figure. At 300 K, the main feature is a weak signal at $g\approx 2$ that we call A. As can be seen, the A line is superimposed on a distorted background. This base line distortion, still visible down to ~ 100 K, is attributed to a second ESR line (called B) which has a linewidth ΔH^B larger than its resonance field H_r^B at $\nu=9.44$ GHz. The spectrum at 80 K appears as a superposition of a narrow line (A) and a broader one (B). Double integration of the 80 K spectrum shows that the intensity of the A signal represents only $\sim 5\%$ of the global intensity. This ESR line should be attributed to an impurity phase or to crystal defects. It is thus tempting to ascribe the broadest component (B signal) to the CBSBr phase. The ESR intensity corresponding to the two observed signals is shown in Fig. 10. The high temperature data on this figure were

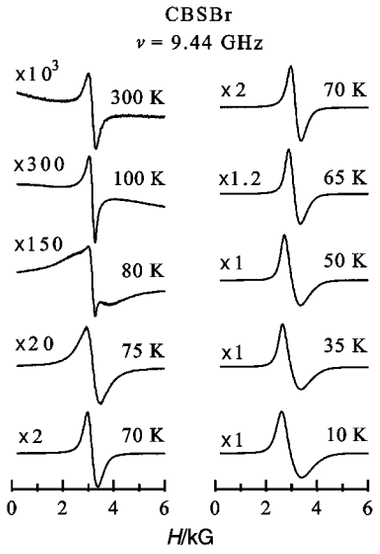

Fig. 9 The same as in Fig. 7 but for CBSBr.

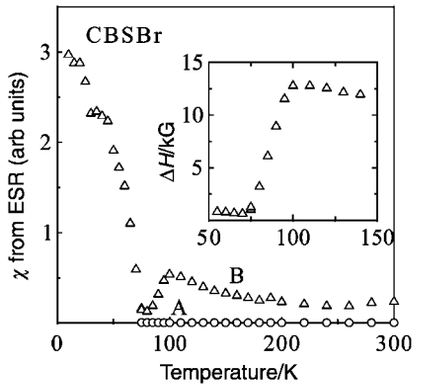

Fig. 10 Absorption intensity corresponding to the CBSBr ESR lines labelled A (circles) and B (triangles) in the text. Inset: temperature dependence of the full width at half maximum of the B line.

obtained by fitting the different spectra using a two lorentzian components model. The high temperature adjustments are certainly very inaccurate because the nominal magnetic field H_{max} is much smaller than the deduced ΔH^B. However, it can be seen when the temperature decreases below 80 K (where $\Delta H^B \leqslant H_{max}$), that the ESR intensity increases abruptly, reproducing quite well the behaviour of the static $\chi(T)$ curve, confirming that the B line is caused by the CBSBr phase. It is also interesting to note that this sudden increase of the intensity is preceded by an anomaly at $\sim$100 K and that a strong linewidth variation also occurs in the same temperature region (inset of Fig. 10). Finally, in the temperature range from 50 to 10 K, where $\chi(T)$ displays a maximum ($T_c = 24.2$ K), it is surprising to see that the asymmetrical B line is little temperature dependent. Given the 300 K crystal structure model proposed in section III, the copper atoms are arranged in trilayers perpendicular to the [001] direction, forming Kagomé type planes separated from each other by a distance of $0.6c \sim 4.37$ Å (CBSBr). The smallest distance between two Cu^{2+} ions belonging to adjacent Kagomé planes is 7.20 Å while the shortest Cu1–Cu1 and Cu1–Cu2 distances within the planes are $\sim$3.19 and $\sim$3.27 Å respectively, making the francisite compounds potentially interesting as low dimensional models. Below the phase transition temperature of $\sim$24.2 K, one enters the domain of ferro (F) or antiferromagnetic (AF) resonance depending on whether the ground state is ferro or antiferromagnetically ordered. If CBSBr is an antiferromagnet at 24.2 K, one should observe, when this temperature is approached from above, a critical broadening of the ESR linewidth caused by the AF fluctuations. On the other hand, if CBSBr is a classical ferromagnet, we expect at its critical temperature T_c a strong exchange narrowing of the ESR line and the opening of a gap in the frequency–field diagram. Since the sample is a powder, the opening of a gap should be accompanied by the appearance of two new resonance lines B′ and B″ lying on each side of the initial B line and moving in opposite directions when the temperature decreases.[13] The B′ mode corresponds to $\boldsymbol{H} \| \boldsymbol{H}_A$ while the B″ one corresponds to $\boldsymbol{H} \perp \boldsymbol{H}_A$, where $\boldsymbol{H}$ and $\boldsymbol{H}_A$ designate the applied and the anisotropy field respectively. We do not observe such a splitting. This suggests that $\boldsymbol{H}_A$ must be very small. In such an anisotropic structure, the low temperature ESR response of CBSBr is therefore surprising. We are planning to further investigate this point in the future.

VII. Conclusion

In this paper, we report a detailed structural study of the francisite compounds $Cu_3Bi(SeO_3)_2O_2X$ (X = Cl, Br, I). Magnetic, optical, and ESR measurements as a function of the temperature are also presented. From the 300 K diffraction data, it is shown that the structure is made of Cu^{2+} trilayers stacked along the c-axis which may realize the $S = 1/2$ Heisenberg model on a Kagomé lattice. This model is of current interest in quantum magnetism because in the case of AF couplings it is highly frustrated and numerical calculations predict that its ground state is a spin liquid. Until now, little could be learnt about this model from the experimental point of view. The list of compounds which effectively realize the AF Heisenberg model on the Kagomé lattice is very short and most of these materials have a spin value greater than 1/2. Concerning the francisite compounds, there is on the basis of the presented data no evidence for a magnetically ordered state at low temperatures. Furthermore, this first magnetic study has also revealed striking features related to the spin dynamics, like for instance i) the absence of Cu^{2+} spin resonance at $\nu = 9.44$ GHz in CBSCl, ii) the anomalous temperature dependence of the ESR linewidth in CBSBr. Synthesis of larger single crystals of the francisite compounds is in progress, for the clarification of these points.

References

1 Von R. Kipka and H. K. Müller-Buschbaum, *Z. Anorg. Allg. Chem.*, 1976, **419**, 58.
2 B. J. Suh, F. Borsa, L. L. Miller, M. Corti, D. C. Johnston and D. R. Torgenson, *Phys. Rev. Lett.*, 1995, **75**, 2212.
3 J. Galy, J. J. Bonnet and S. Andersson, *Acta Chem. Scand. A*, 1979, **33**, 383.
4 B. Bastide, P. Millet, M. Johnsson and J. Galy, *Mater. Res. Bull.*, 2000, **35**, 847.
5 P. Millet, B. Bastide and M. Johnsson, *Solid State Commun.*, 2000, **113**, 719.
6 S. V. Krivovichev, R. R. Shuvalov, T. F. Semenova and S. K. Filatov, *Z. Kristallogr.*, 1999, **214**, 135.
7 S. V. Krivovichev, S. K. Filatov, T. F. Semenova and I. V. Rozhdestvenskaya, *Z. Kristallogr.*, 1998, **213**, 645.
8 A. Pring, B. M. Gatehouse and W. D. Birch, *Am. Mineral.*, 1990, **75**, 1421.
9 "Collect" data collection software, Nonius B. V., 1998.
10 A. Altomare, G. Cascarano, C. Giacovazzo, A. Cuagliardi, M. C. Burla, A. Polidori and M. Camalli, *J. Appl. Crystallogr.*, 1994, **27**, 435.
11 G. M. Sheldrick, SHELXL-97, Program for the Refinement of Crystal Structures, University of Göttingen, Germany, 1997.
12 R. H. Blessing, *J. Appl. Crystallogr.*, 1997, **30**, 421.
13 F. Reynaud, A. M. Ghorayeb, Y. Ksari, N. Menguy, A. Stepanov and C. Delmas, *Eur. Phys. J. B*, 2000, **14**, 83.